Chapter 4
Planar Joints with Clearance: Dry Contact Models

In general, a multibody system is made of several components, which can be divided into links with a convenient geometry and joints, which introduce restrictions on the relative motion of the various bodies of the system (Shabana 1989). Usually the links are modeled as rigid or deformable bodies, while the joints are modeled through a set of kinematic constraints, that is, the joints are not modeled *de per si* (Bauchau and Rodriguez 2002). The functionality of a kinematic joint relies upon the relative motion allowed between the connected components, which, in practice, implies the existence of a gap, that is, a clearance between the mating parts, leading to surface contact, shock transmission and the development of different regimes of friction and wear. No matter how small the clearance is, it can lead to vibration and fatigue phenomena, lack of precision or, in the limit, to even random overall behavior. If there is no lubricant or other damping materials in the joint, impacts occur in the system and the corresponding impulses are transmitted throughout the multibody system. In this work, the elements that compose the clearance joints are modeled as colliding bodies. The impact between the two bodies is treated as a continuous event, that is, the local deformations and the contact forces are continuous functions of time. The impact analysis of the system is performed simply by including the contact-impact forces in the equations of motion during the impact period (Flores and Ambrósio 2004). From the system configuration, a geometric condition defines if the elements of the joints are in contact or not. Thus the dynamics of joints with clearances is controlled by contact-impact forces, rather than by the kinematic constraints of the ideal joints. A force model that accounts for the geometric and material characteristics of the clearance joint components describes these impacts and the eventual continuous contact (Lankarani and Nikravesh 1990). The energy dissipative effects are introduced in the joints through the contact force model and by friction forces that develop during the contact (Ambrósio 2002). The main purpose of this chapter is to present the mathematical models for revolute and translational joints with clearance in planar multibody mechanical systems. The methodologies and procedures adopted in this chapter are applied to a slider–crank mechanism, which includes both revolute and translational joints with clearance. For the case of revolute joints with clearance, the contact force models presented in the previous chapter are used to assess the influence of the different models on the impact force.

P. Flores et al., *Kinematics and Dynamics of Multibody Systems with Imperfect Joints.*

4.1 Clearance Models

It is known that the performance of a multibody system is degraded by the presence of clearances in the joints because impact forces occur. These impact forces contribute to the failure of the components due to shock loading, reducing the systems' life due to material fatigue, generating high noise levels, causing energy dissipation and exciting unwanted vibratory responses (Dubowsky and Freudenstein 1971a,b, Ravn 1998, Flores and Ambrósio 2004, Flores et al. 2006).

In standard multibody models, it is assumed that the connecting points of two bodies, linked by an ideal or perfect revolute joint, are coincident. The introduction of the clearance in a revolute joint allows for the separation of these two points. Figure 4.1 depicts a revolute joint with clearance, that is, the so-called journal–bearing, where the difference in radius between the bearing and the journal defines the radial clearance.

Although a revolute joint with clearance does not constrain any degree of freedom from the mechanical system, as the ideal joint does, it imposes some kinematic restrictions, limiting the journal to move within the bearing. Thus, when the clearance is present in a planar revolute joint, two kinematic constraints are removed and two degrees of freedom are introduced instead. The dynamics of the joint is then controlled by contact-impact forces between the journal and the bearing. Thus, whilst a perfect revolute joint in a mechanical system imposes kinematic constraints, a revolute clearance joint leads to force constraints. Therefore mechanical joints with clearance can be defined as force-joints instead of kinematic joints.

In a revolute clearance joint, when contact exists between the journal and the bearing, a contact-impact force, perpendicular to the plane of collision, develops. The force is typically applied as a spring–damper element. If this element is linear, the approach is known as the Kelvin–Voigt model (Timoshenko and Goodier 1970). If the relation is nonlinear, the model is generally based on the Hertz contact law (Hertz 1896).

In what concerns the clearance modeling, there are, in general, three different approaches, namely, the massless link approach, the spring–damper approach and the

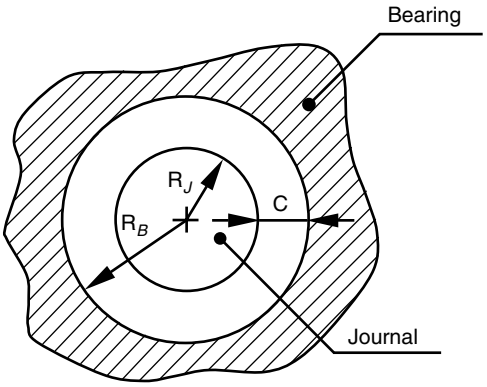

Fig. 4.1 Revolute joint with clearance, that is, the so-called journal–bearing

momentum exchange approach. The massless link approach (Earles and Wu 1975), in which the presence of clearance at a joint is modeled by adding an imaginary massless link with a fixed length equal to the clearance, is illustrated in Fig. 4.2a. This link results in the mechanism model having an additional degree of freedom. Hence the resulting equations of motion are found to be highly nonlinear and complex to solve. Furthermore this model assumes that there is contact between the journal and the bearing all the time, hence unable to represent free flight trajectories. Wu and Earles (1977) used the massless link model to predict the occurrence of contact loss in revolute joints of planar mechanisms.

The spring–damper approach (Dubowsky and Freudenstein 1971a,b, Bengisu et al. 1986), in which the clearance is modeled by introducing a spring–damper element that simulates the surface elasticity, is in Fig. 4.2b. This model shows some deficiencies in representing the physical nature of the energy transfer during the impact process, the parameters of the spring and damper elements being difficult to quantify. Dubowsky (1974) investigated the dynamic effects of clearance in planar mechanisms by simulating the elasticity of the contacting surfaces using linear springs and dampers.

In the momentum exchange approach (Townsend and Mansour 1975, Ravn 1998, Flores et al. 2006), the mechanical elements that constitute a clearance joint are considered as impacting bodies. The contact-impact forces control the dynamics of the clearance joint. The work presented in this book uses methodologies that are in line with momentum exchange approach in the kinematics of the contacting bodies concerned. In the massless link and spring–damper models, the clearance is replaced by mechanical components, which are intended to represent the behavior of the clearance as closely as possible. The momentum exchange approach is more realistic since the impact force model allows, with high level of approximation, to simulate the elasticity of the contacting surfaces as well as the energy dissipation during the impact.

Several published works focused on the different modes of motion of the journal inside the bearing. Most of these consider a three-mode model for predicting the dynamical response of articulated systems with revolute clearance joints (Mansour and Townsend 1975, Miedema and Mansour 1976). The three different modes of journal motion inside the bearing are the contact or following mode, the free flight

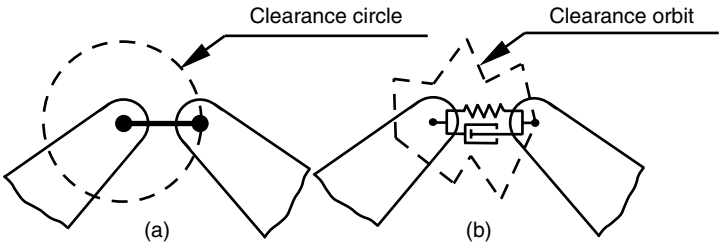

Fig. 4.2 Examples of models for revolute joints with clearance: (**a**) massless link model; (**b**) spring–damper model

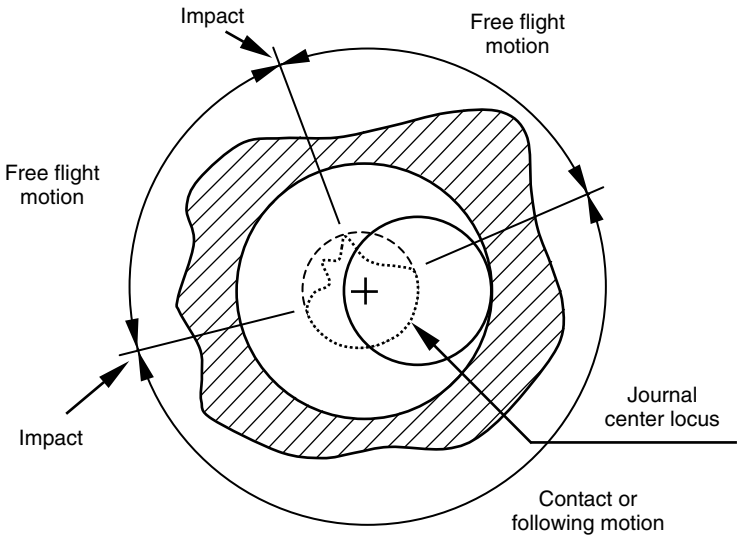

Fig. 4.3 Types of journal motion inside the bearing

mode and the impact mode. These three types of the journal motion are illustrated in Fig. 4.3.

In the contact or following mode, the journal and the bearing are in permanent contact and a sliding motion between the contacting surfaces exists. In this mode, the relative penetration depth varies along the circumference of the bearing. This mode ends when the journal and the bearing separate from each other, and the journal enters the free flight mode. In the free flight mode, the journal can move freely inside the bearing boundaries, that is, the journal and the bearing are not in contact and, consequently, no reaction force develops at the joint. In the impact mode, which occurs on the termination of the free flight mode, impact forces are applied to the system. This mode is characterized by a discontinuity in the kinematic and dynamic characteristics, and a significant exchange of momentum occurs between the two impacting bodies. At the termination of the impact mode, the journal can enter either a free flight or a following mode. During the dynamic simulation of a revolute joint with clearance, if the path of the journal center is plotted for each instant, these different modes of motion, depicted in Fig. 4.3, can be easily identified.

4.2 Model of Revolute Joint with Clearance

The simulation of real joints requires the development of a mathematical model for revolute clearance joints in the multibody systems. Figure 4.4 shows two bodies i and j connected by a generic revolute joint with clearance. Part of body i is the bearing and part of body j is the journal. The center of mass of bodies i and j are O_i and O_j, respectively. Body-fixed coordinate systems $\xi\eta$ are attached to the

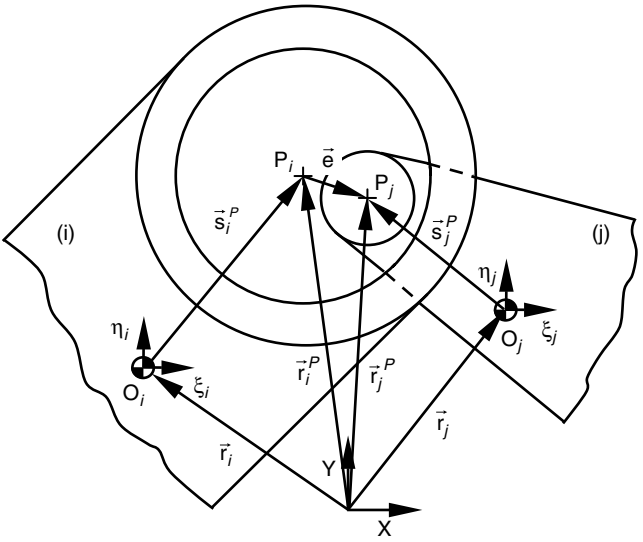

Fig. 4.4 Generic revolute joint with clearance in a multibody system

center of mass of each body, while the XY coordinate frame represents the global coordinate system. Point P_i indicates the center of the bearing, and the center of the journal is denominated by point P_j.

In the dynamic simulation, the behavior of the revolute clearance joint is treated as an oblique eccentric impact between the journal and the bearing. The mechanics of this type of impact involves both the relative normal velocity and the relative tangential velocity (Zukas et al. 1982). When the impact occurs, an appropriate contact law must be applied, the resulting forces being introduced in the system equations of motion as generalized forces.

Taking into account Fig. 4.4, the eccentricity vector **e** connecting the centers of the bearing and the journal is calculated as

$$\mathbf{e} = \mathbf{r}_j^P - \mathbf{r}_i^P \tag{4.1}$$

where both $\mathbf{r}_i^P$ and $\mathbf{r}_j^P$ are described in the global coordinates reference frame as (Nikravesh 1988)

$$\mathbf{r}_k^P = \mathbf{r}_k + \mathbf{A}_k \mathbf{s}_k'^P, \, (k = i, \, j) \tag{4.2}$$

The magnitude of the eccentricity vector is evaluated as

$$e = \sqrt{\mathbf{e}^{\mathrm{T}} \mathbf{e}} \tag{4.3}$$

where $\mathbf{e}^T$ is the transpose of vector **e**.

The unit normal vector **n** to the surfaces in collision between the bearing and the journal, designated as **n**, is aligned with the eccentricity vector:

$$\mathbf{n} = \mathbf{e}/e \tag{4.4}$$

The unit vector is aligned with the line between the centers of the bearing and the journal.

With reference to Fig. 4.5, the penetration depth caused by the impact between the journal and the bearing is evaluated as

$$\delta = e - c \tag{4.5}$$

where c is the radial clearance, defined as the difference between the radius of the bearing and the radius of the journal.

Let points Q_i and Q_j represent the contact points on bodies i and j, respectively. The position of the contact points Q_i and Q_j are evaluated as

$$\mathbf{r}_k^Q = \mathbf{r}_k + \mathbf{A}_k \mathbf{s}_k'^Q + R_k \mathbf{n}, \ (k = i, j) \tag{4.6}$$

where R_i and R_j are the bearing and journal radiis, respectively.

In some contact models, it is important to evaluate the dissipative effects that develop during impact. In the continuous force contact model it, is necessary to calculate the relative velocity between the impacting surfaces. The velocity of the contact points Q_i and Q_j in the global coordinate system is found by differentiating (4.6) with respect to time, i.e.,

$$\dot{\mathbf{r}}_k^Q = \dot{\mathbf{r}}_k + \dot{\mathbf{A}}_k \mathbf{s}_k'^Q + R_k \dot{\mathbf{n}} \tag{4.7}$$

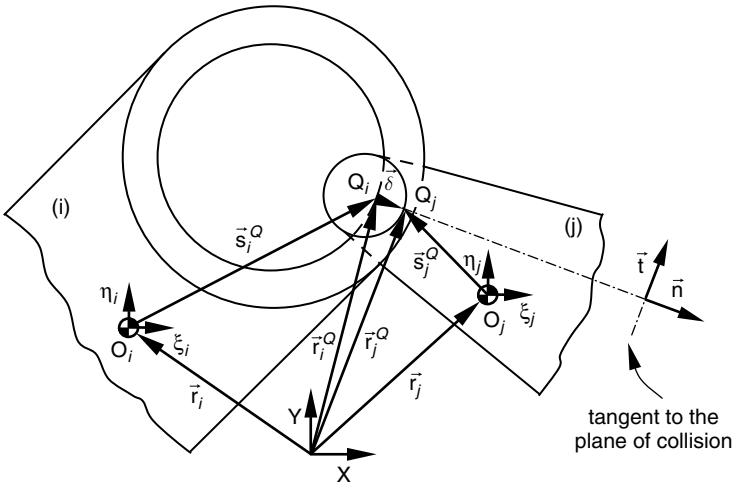

Fig. 4.5 Penetration depth due to the impact between the bearing and the journal

where $(\dot{\bullet})$ denotes the derivative with respect to time of quantity $(\bullet)$.

The relative velocity between the contact points is projected onto the tangential line to the colliding surfaces and onto the normal to colliding surfaces, yielding a relative tangential velocity, $\mathbf{v}_T$, and a relative normal velocity, $\mathbf{v}_N$, shown in Fig. 4.6. The normal relative velocity determines whether the contact bodies are approaching or separating. The tangential relative velocity determines whether the contact bodies are sliding or sticking. The relative scalar normal and tangential velocities are

$$v_N = (\dot{\mathbf{r}}_j^Q - \dot{\mathbf{r}}_i^Q)^T \mathbf{n} \tag{4.8}$$

$$v_T = (\dot{\mathbf{r}}_j^Q - \dot{\mathbf{r}}_i^Q)^T \mathbf{t} \tag{4.9}$$

where $\mathbf{t}$ is obtained by rotating the vector $\mathbf{n}$, calculated using (4.4), in the counter clockwise direction by 90°.

The normal and tangential forces, $\mathbf{f}_N$ and $\mathbf{f}_T$, respectively, are applied at the contact points. These forces are evaluated using the contact force law proposed in Chap. 3 and a friction model such as the Coulomb law. The contributions to the generalized vector of forces and moments, $\mathbf{g}$ in the equation of motion, are found by projecting the normal and tangential forces onto the X and Y directions. These forces that act on the contact points of bodies i and j are transferred to the center of mass of bodies and an equivalent transport moment is applied to the rigid body. Referring to Fig. 4.7, the forces and moments that act on the center of mass of body i due to the clearance joint contact are given by

$$\mathbf{f}_i = \mathbf{f}_N + \mathbf{f}_T \tag{4.10}$$

$$m_i = -(y_i^Q - y_i) f_i^x + (x_i^Q - x_i) f_i^y \tag{4.11}$$

The corresponding forces and moments applied to the body j are

$$\mathbf{f}_j = -\mathbf{f}_i \tag{4.12}$$

$$m_j = (x_j^Q - x_j) f_j^y - (y_j^Q - y_j) f_j^x \tag{4.13}$$

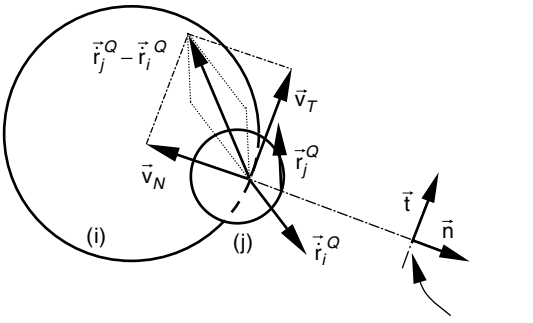

Fig. 4.6 Velocity vectors of impact between the bearing and the journal

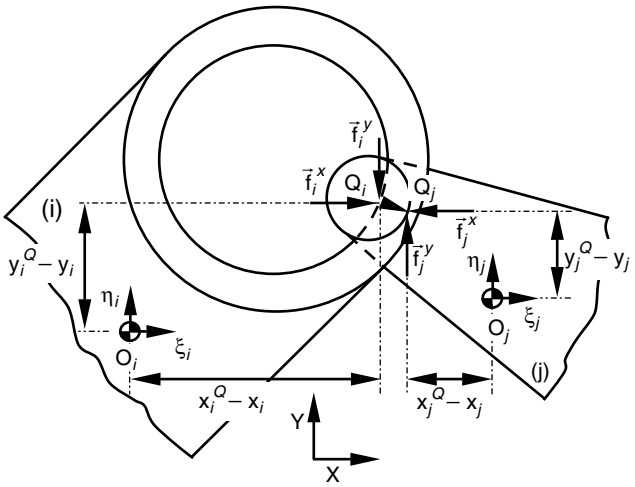

Fig. 4.7 Force vectors that act at the points of contact

4.3 Model of Translational Joint with Clearance

Similar to the procedure used in the previous section for the revolute joint, this presents a mathematical model for translational joints with clearance in multibody systems. Figure 4.8 shows an example of a planar translational joint with clearance. The clearance c is defined as the difference between the guide and slider surfaces. The geometric characteristics of the translational clearance joint used here are the length of the slider L, the slider width W and the distance between the guide surfaces H. In the present work, the slider and the guide elements that constitute a translational clearance joint are modeled as two colliding bodies and the dynamics of the joint is governed by contact-impact forces. The equations of motion that govern the dynamic response of the general multibody systems incorporate these forces.

In an ideal translational joint the two bodies, slider and guide, translate with respect to each other along the line of translation, so that there is neither rotation between the bodies nor a relative translation motion in the direction perpendicular to the axis of the joint. Therefore an ideal translational joint reduces the number

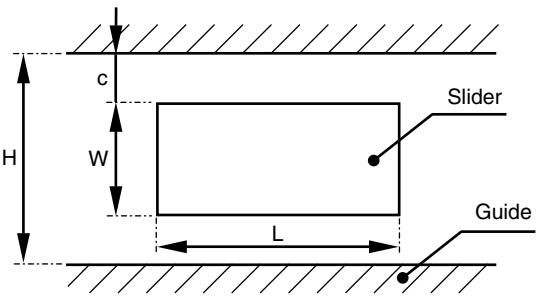

Fig. 4.8 Translational joint with clearance, that is, the slider and its guide

of degrees of freedom of the system by two. The existence of a clearance in a translational joint removes the two kinematic constraints and introduces two extra degrees of freedom. Hence the slider can move 'freely' inside the guide limits. When the slider reaches the guide surfaces an impact occurs and the dynamic response of the joint is controlled by contact forces. These contact forces are evaluated according to the continuous contact force proposed together with the dissipative friction force model selected. Then these forces are introduced into the system equations of motion as external generalized forces. Although a translational clearance joint does not constrain any degree of freedom from the mechanical system, as an ideal joint does, it imposes some restrictions on the slider motion inside the guide. Thus, while a perfect joint in a multibody system is achieved by kinematic constraints, a clearance joint is obtained by force constraints.

Over the last few decades extensive work has been done to study the dynamic effect of the revolute clearance in multibody systems (Dubowsky and Freudenstein 1971a, Ravn 1998, Schwab 2002, Flores and Ambrósio 2004). In contrast, little work has been done to model translational joints with clearance. Wilson and Fawcett (1974) derived the equations of motion for the different scenarios of the slider motion inside the guide. They also showed how the slider motion in a translational clearance joint depends on the geometry, speed and mass distribution. Farahanchi and Shaw (1994) studied the dynamic response of a planar slider–crank mechanism with slider clearance. More recently, Thümmel and Funk (1999) used the complementary approach to model impact and friction in a slider–crank mechanism with both revolute and translational clearance joints.

The modeling of translational clearance joints is more complicated than that for the revolute joints, due to the several possible contact configurations between the slider and the guide. Figure 4.9 illustrates four different scenarios for the slider configuration relative to guide surface, namely: (1) no contact between the two elements: the slider is in free flight motion inside the guide and, consequently, there is no reaction force at the joint; (2) one corner of the slider is in contact with the guide surface; (3) two adjacent slider corners are in contact with the guide surface, which corresponds to having a face of slider in contact with the guide surface; (4) two opposite slider corners are in contact with the guide surface. The conditions for switching between different cases depend on the system's dynamics. For the cases represented in Fig. 4.9, the contact forces are evaluated using the continuous contact force model.

In order for the clearance joints to be simulated in the multibody system environment, it is required that a mathematical model be developed. Figure 4.10 shows a representation of a translation joint with clearance that connects bodies i and j. The slider is body i whereas the guide is part of body j. The center of mass of bodies i and j are O_i and O_j, respectively. Let points P, Q, R and S in the guide surfaces indicate the geometric limits inside which contact may occur. Points A_i,B_i, C_i andD_i indicate the four corners of the slider, and A_j, B_j, C_j and D_j are the points on the guide surfaces that are closer to the points in body j. The contact formulation for all corners in the slider is similar, and therefore, in what follows only the slider corner A is used to describe the mathematical formulation.

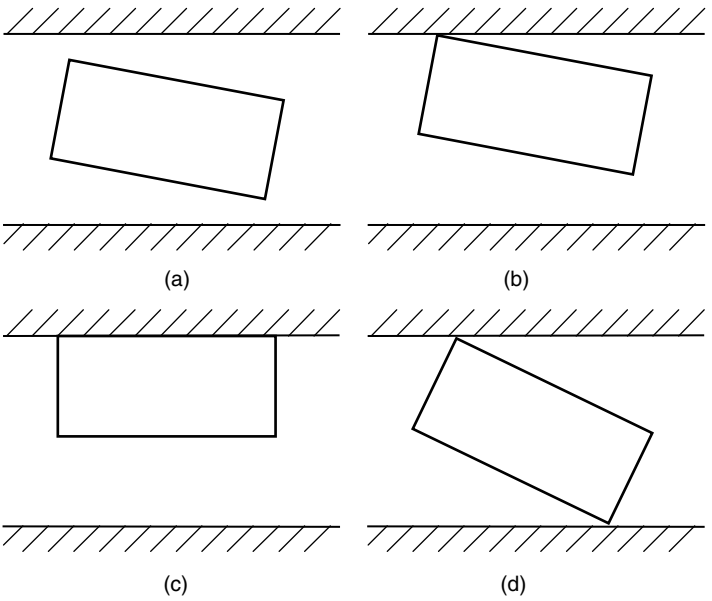

Fig. 4.9 Different scenarios for the slider motion inside the guide: (**a**) no contact; (**b**) one corner in contact with the guide; (**c**) two adjacent corners in contact with the guide; (**d**) two opposite corners in contact with the guide

Let vector $\mathbf{t}$, directed along the guide surface from point P to point Q in body j, be written in terms of the body-fixed coordinates as

$$\mathbf{t'}_j = \mathbf{s'}_j^Q - \mathbf{s'}_j^P \tag{4.14}$$

Note that the tangent vector expressed in the inertia frame is $\mathbf{t} = \mathbf{A}_j \mathbf{t}'$, where $\mathbf{A}_j$ is the transformation matrix from body j's frame to the inertial frame.

Let the position vector for any given point G of a body k be described with respect to inertial reference frame as

$$\mathbf{r}_k^G = \mathbf{r}_k + \mathbf{A}_\kappa \mathbf{s'}_k^G, (k = i, j) \tag{4.15}$$

where $\mathbf{s'}_k^G$ is the position of point G in body k expressed in body-fixed coordinates.

The position of point A_j, belonging to the segment PQ of the guide, closest to point A_i located in the corner of the slider, is given as

$$\mathbf{r}_j^A = \mathbf{r}_j^P + [\mathbf{t}^T(\mathbf{r}_i^A - \mathbf{r}_j^P)]\mathbf{t} \tag{4.16}$$

The vector connecting the slider corner A_i to point A_j on the guide surface is

$$\boldsymbol{\delta} = \mathbf{r}_j^A - \mathbf{r}_i^A \tag{4.17}$$

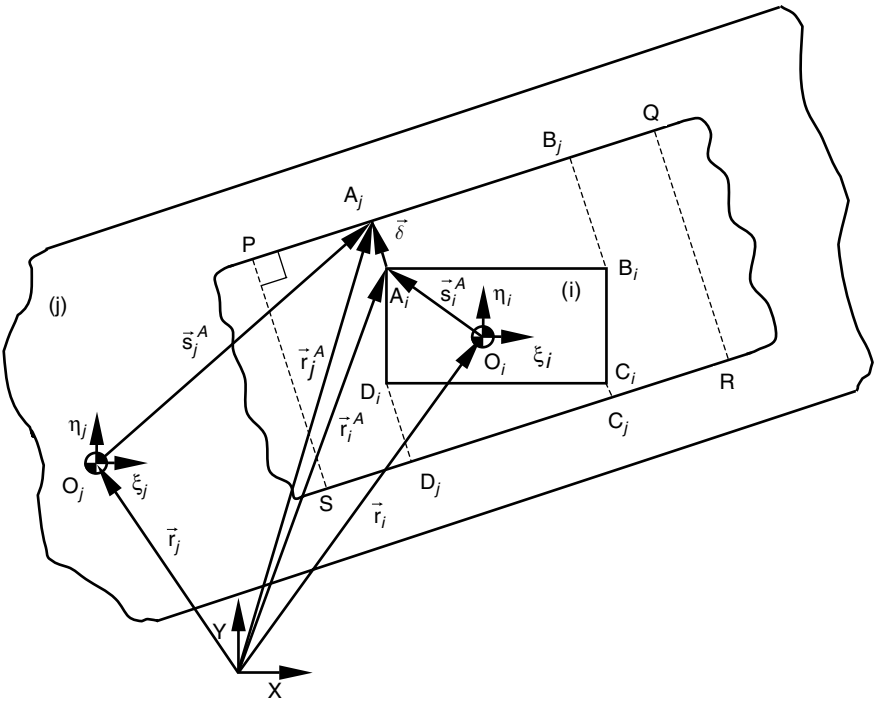

Fig. 4.10 Generic translational clearance joint in a multibody system

Note that vector $\boldsymbol{\delta}$ has the same direction as the normal $\mathbf{n}$ to the guide surface. Regardless of this identity, let the normal vector $\mathbf{n}$ be defined as perpendicular to the tangent vector $\mathbf{t}$, which for two-dimensional cases is

$$\mathbf{n} = [\, t_y \; -t_x \,]^T \tag{4.18}$$

Figure 4.11 shows the slider and guide in two different scenarios, namely in a noncontact situation and in the case of penetration between the slider and guide surface. For the contact case, the vectors $\boldsymbol{\delta}$ and $\mathbf{n}$ are parallel but oriented in opposite directions. Thus the condition for penetration between the slider and guide is expressed as

$$\mathbf{n}^T \boldsymbol{\delta} < 0 \tag{4.19}$$

The magnitude of the penetration depth for point A_i is evaluated as

$$\delta = \sqrt{\boldsymbol{\delta}^T \boldsymbol{\delta}} \tag{4.20}$$

The impact velocity, required for the evaluation of the contact force, is obtained by differentiating (4.17) with respect to time, yielding

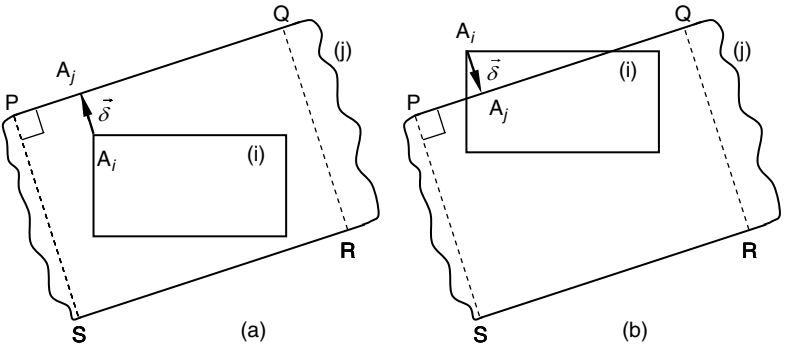

Fig. 4.11 (**a**) Noncontact situation; (**b**) penetration between the slider corner A and the guide surface

$$\dot{\boldsymbol{\delta}} = \dot{\mathbf{r}}_j + \dot{\mathbf{A}}_j \mathbf{s}'^{A}_j - \dot{\mathbf{r}}_i - \dot{\mathbf{A}}_i \mathbf{s}'^{A}_i \tag{4.21}$$

When the contact between the slider and the guide surfaces takes place, normal and tangential forces appear in the contact points. By transferring these forces to the center of mass of each body Fig. 4.12 shows the forces and moments acting on the center of mass of body I, which are

$$\mathbf{f}_i = \mathbf{f}_N + \mathbf{f}_T \tag{4.22}$$

$$m_i = -(y_i^Q - y_i) f_i^x + (x_i^Q - x_i) f_i^y \tag{4.23}$$

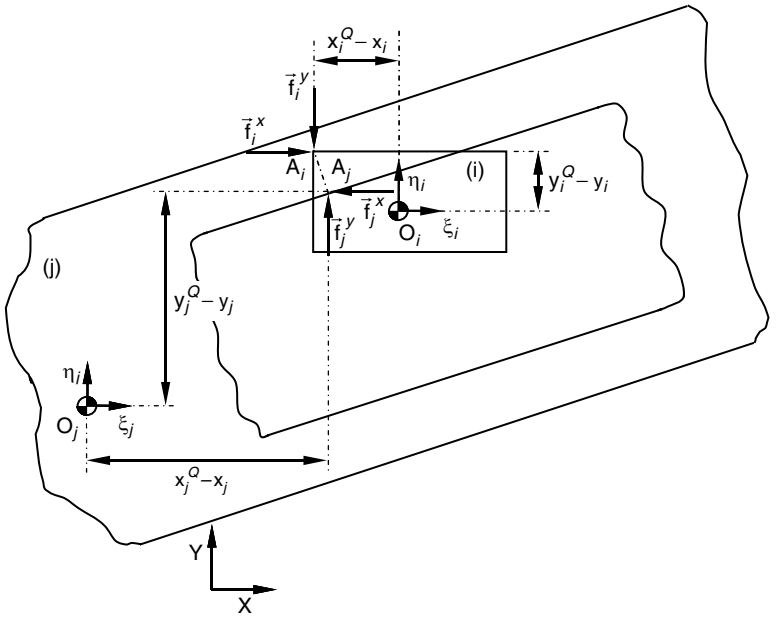

Fig. 4.12 Forces that act at the points of contact between the slider and the guide

The forces and moments to be applied in body j are written as

$$\mathbf{f}_j = -\mathbf{f}_i \tag{4.24}$$

$$m_j = (x_j^Q - x_j) f_j^y - (y_j^Q - y_j) f_j^x \tag{4.25}$$

In dealing with translational clearance joints, it is essential to define how the slider and guide surfaces contact each other and, consequently, what is the most adequate contact force model. Lankarani (1988) presented a linear model for contact between two square plane surfaces as

$$F_N = K\delta \tag{4.26}$$

where the stiffness parameter K is given by

$$K = \frac{a}{0.475(\sigma_i + \sigma_j)} \tag{4.27}$$

having the area of contact a length of $2a$ and quantities σ_i and σ_j are given by (3.4).

When two adjacent slider corners contact with the guide surface, the resulting contact force is applied at the geometric center of the penetration area, denoted as GC in Fig. 4.13a, and the contact force model given by (4.26) is used. Otherwise, when one or two opposite slider corners contact the guide surface the contact is assumed to be between a spherical surface and a plane surface, allowing for the contact model given by Hertz law with hysteretic damping factor expressed by (3.9) to be applied. In order to evaluate the equivalent stiffness, a small curvature radius R_c is assumed on the contact corner, represented in Fig. 4.13b. The unified contact model is obtained using the pseudo-stiffness expressed by (4.27) in the continuous force model represented by (3.9).

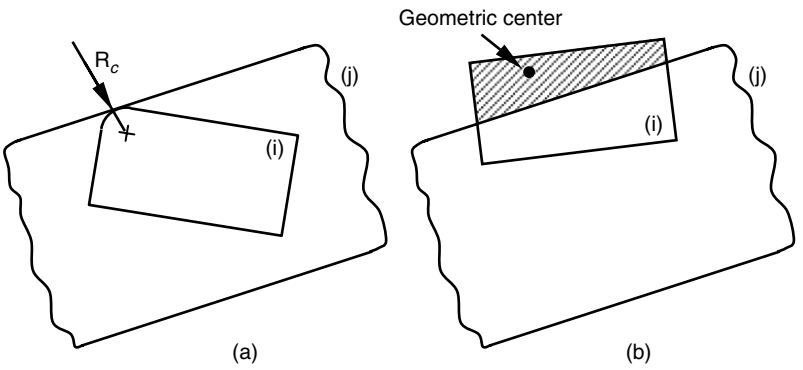

Fig. 4.13 (**a**) Contact between a spherical surface and a plane; (**b**) contact between two plane surfaces

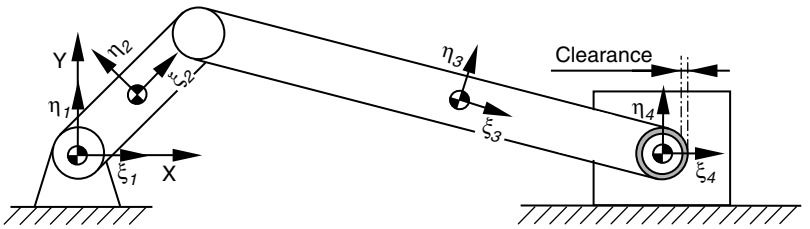

Fig. 4.14 Slider–crank mechanism with a revolute clearance joint

4.4 Application 1: Slider–Crank with Revolute Clearance Joint

The slider–crank mechanism is chosen as an example to demonstrate the application of the methodologies presented in this chapter. The same mechanism has been studied by other authors (Ravn 1998, Schwab 2002), which allows the comparison of the results obtained. Figure 4.14 shows the configuration of the slider–crank mechanism, which consists of four rigid bodies, two ideal revolute joints and one ideal translational joint. A revolute clearance joint exists between the connecting rod and the slider.

The crank, which is the driving link, rotates with a constant angular velocity of 5000 rpm. The initial configuration of the mechanism is defined with the crank and the connecting rod collinear and the journal and bearing centers coincident. Furthermore the initial positions and velocities necessary to start the dynamic analysis are obtained from kinematic simulation of the slider–crank mechanism in which all the joints are considered to be ideal. The geometric and inertia properties of each body are listed in Table 4.1. The parameters used for the different models, required to characterize the problem, and for the numerical methods, required to solve the system dynamics, are listed in Table 4.2.

The dynamic response of the slider–crank mechanism is obtained and represented in Figs. 4.15 and 4.16 by the time plots of the velocity and acceleration of the slider and the moment acting on the crank, which is required to maintain the crank angular velocity constant. The relative motion between journal and bearing centers is plotted in Figs. 4.15d and 4.17. The Hertz contact force law with hysteretic damping factor, given by (3.9), is used to evaluate the contact force between the journal and bearing. Figure 4.15 shows the results for the case in which the clearance size is 0.5 mm. Note that the results, reported for the two full crank rotations after steady-state has been reached, are plotted against those obtained for an ideal joint.

In Fig. 4.15a, it is observed that the existence of a joint clearance influences the slider velocity by leading to a staircase-like behavior. The periods of constant

Table 4.1 Geometric and inertia properties of the slider–crank mechanism

Body nr	Length (m)	Mass (kg)	Moment of inertia (kg m^2)
2	0.05	0.30	0.00010
3	0.12	0.21	0.00025
4	–	0.14	0.00010

Table 4.2 Parameters used in the dynamic simulation of the slider–crank mechanism with revolute clearance joint

Bearing radius	10.0 mm	Baumgarte - α	5
Restitution coefficient	0.9	Baumgarte - β	5
Young's modulus	207 GPa	Integration step	10^{-5} s
Poisson's ratio	0.3	Integration tolerance	10^{-6} s

velocity observed for the slider mean that the journal moves freely inside the bearing boundaries. The sudden changes in velocity are due to the impact between the journal and the bearing. When a smooth change in the velocity curve of the slider is observed it indicates that the journal and the bearing are in continuous contact, that is, the journal follows the bearing wall. This situation is confirmed by smooth changes in the acceleration curve. The slider acceleration exhibits high peaks caused by impact forces that are propagated through the rigid bodies of the mechanism, as perceived in Fig. 4.15b where the acceleration of the slider is displayed. The slider acceleration presents high peaks of its values, which may be smoothed in a real mechanism due to the energy dissipation associated with the system components' flexibility. The same phenomena can be observed in the crank moment, represented by Fig. 4.15c. As far as the trajectory of the journal center relative to the bearing center is concerned, different types of motion between the two bodies can be

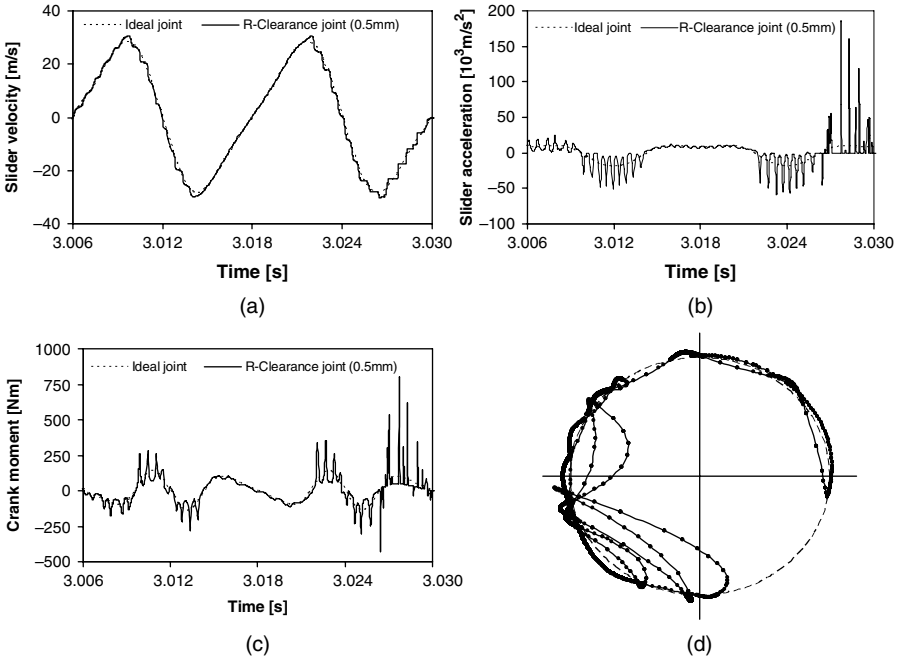

Fig. 4.15 (**a**) Slider velocity; (**b**) slider acceleration; (**c**) crank moment required to maintain its angular velocity constant; (**d**) journal trajectory relative to the bearing

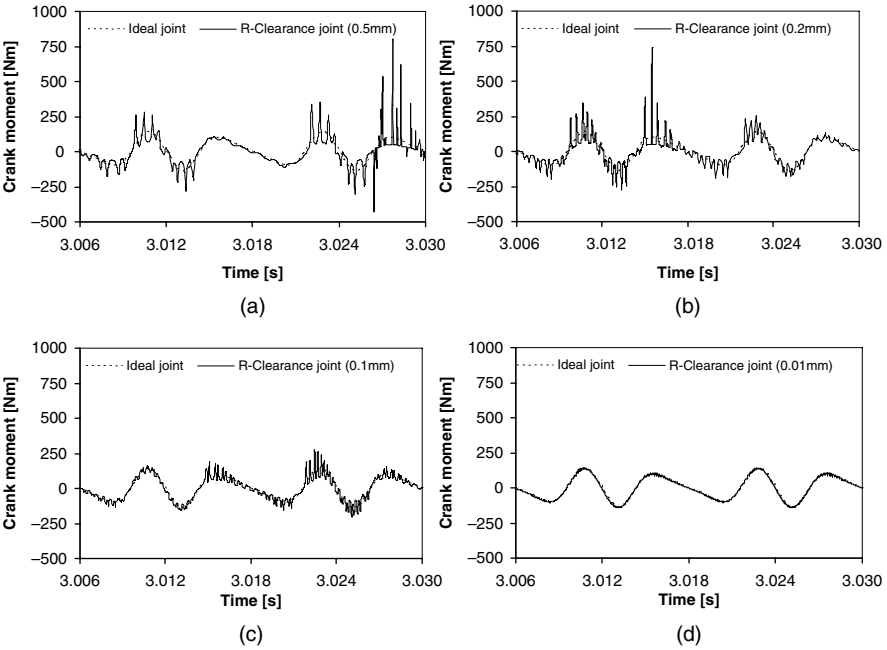

Fig. 4.16 Crank moment for different radial clearance sizes: (**a**) $c = 0.5$ mm; (**b**) $c = 0.2$ mm; (**c**) $c = 0.1$ mm; (**d**) $c = 0.01$ mm

observed, namely, free flight, impact and rebound, and permanent or continuous contact. The relative penetration depth between the journal and the bearing is visible by the points of the journal that are plotted outside the clearance circle, in Fig. 4.15d, where the journal center trajectories are presented by continuous lines that connect point markers. Each one of the markers represents the position of the journal for a given time step. It can be observed that during the free flight motion the time step adopted by the integration algorithm is much larger than during the contact. When contact is detected, the integration time step decreases significantly, which shows the importance of varying time-step integration algorithm for problems involving contact.

The clearance size is one of the most important parameters that affect the dynamic behavior of the system. In Figs. 4.16–4.18, the crank moments, the journal center trajectories and the Poincaré maps are used to illustrate the dynamic behavior of the slider–crank mechanism when different clearance sizes are present. In this application, the slider acceleration and slider velocity are chosen to plot the Poincaré maps. The values for the clearance of the revolute joint are chosen to be 0.5, 0.2, 0.1 and 0.01 mm.

Poincaré maps are mathematical abstractions which are often useful in highlighting the dynamic behavior of systems in terms of periodic, quasi-periodic and chaotic motion. Especially chaotic systems are often examined through the use of Poincaré maps. A Poincaré map consists of plotting the value of two components

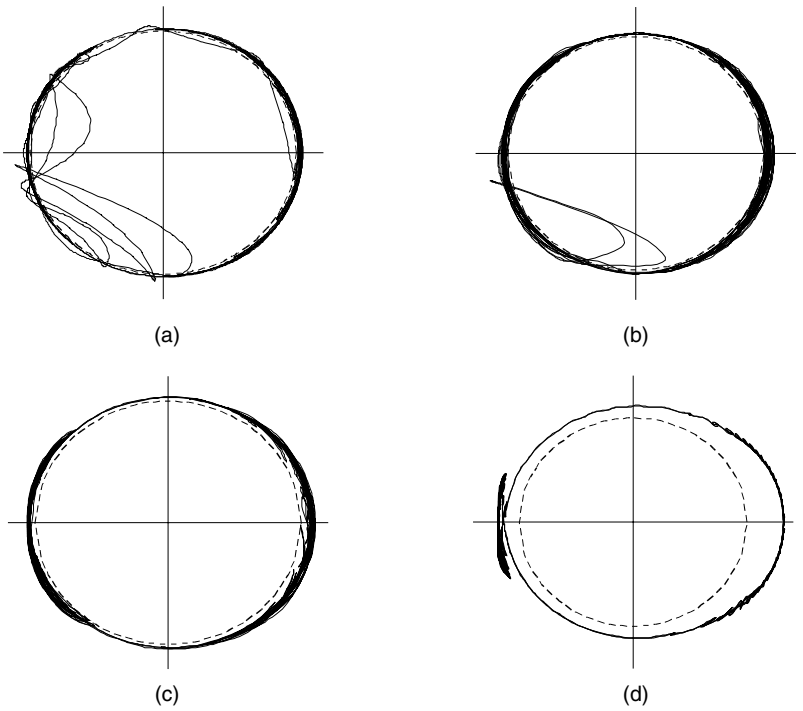

Fig. 4.17 Journal center trajectory with respect to the bearing for different radial clearance sizes, the maximum eccentricity being plotted with a *dashed circle*: (**a**) $c = 0.5$ mm; (**b**) $c = 0.2$ mm; (**c**) $c = 0.1$ mm; (**d**) $c = 0.01$ mm

from the state vector versus its derivative, i.e., $\mathrm{y}(t)$ and $\dot{y}(t)$ (Baker and Gollub 1990, Tomsen 1997). Regular or periodic behavior is insensitive to initial conditions and is represented in the Poincaré map by a closed orbit or finite number of points. Chaotic or nonperiodic responses are extremely sensitive to initial conditions and are perceived by a region densely filled by orbits or points in the Poincaré map. A complicated looking phase in a Poincaré map is one indicator of chaotic motion. Quasi-periodic orbits fill up the Poincaré maps as the chaotic orbits, but they do so in a fully predictable manner since there is not such a sensitive dependency on the initial conditions (Wiggins 1990).

From the Poincaré maps analysis, the slider–crank mechanism behavior can easily be characterized, and it is possible to distinguish between periodic, quasi-periodic and chaotic responses. In multibody systems, nonlinearities arise from intermittent motion, clearance joints, friction effect and contact forces, among others. The relation between the clearance size and the type of motion observed is clearly identified from plots in Fig. 4.18.

Figure 4.16 shows that when the clearance size is decreased the dynamic behavior tends to be smoother, which is represented by lower peaks in the crank moment. Indeed, when the clearance is small, the system response tends to be closer to the ideal

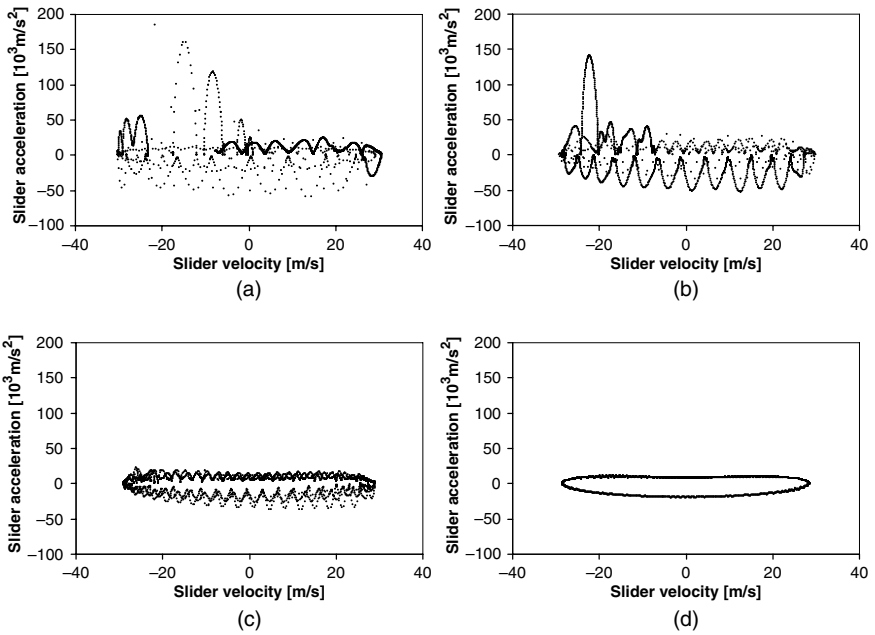

Fig. 4.18 Poincaré maps for different radial clearance sizes: (**a**) $c = 0.5$ mm; (**b**) $c = 0.2$ mm; (**c**) $c = 0.1$ mm; (**d**) $c = 0.01$ mm

response meaning that the journal and the bearing experiment a smaller number of impacts. Hence the clearance joint behavior tends to be periodic instead of nonlinear or chaotic. This conclusion is easily confirmed by the journal center trajectories and the respective Poincaré maps displayed in Fig. 4.17d and 4.18d, respectively. Figure 4.17a and b clearly shows a nonperiodic motion between the journal and bearing since it does not repeat from cycle to cycle. This is confirmed by the respective Poincaré map displayed in Fig. 4.18a and b, where the chaotic behavior can be clearly observed. This chaotic response suggests that impacts followed by some rebounds take place. Figure 4.18c shows a quasi-periodic motion, because the orbits fill up the Poincaré maps in a fully predictable manner, thus there is no sensitive dependence on the initial conditions. It is clear that, when the clearance is reduced, the dynamic response tends to be periodic or regular, which indicates that the journal follows the bearing wall. It is noteworthy that, for an ideal revolute joint, the Poincaré map is almost the same as the map shown in Fig. 4.18d, which is expected in so far as all the bodies in the system exhibit a periodic motion.

In a way similar to the clearance size study for the crank moments, the journal center trajectories and Poincaré maps are used to quantify the behavior of the slider–crank mechanism when friction is taken into account. In the models used, the contact between the journal and the bearing is modeled by the Lankarani and Nikravesh force model, given by (3.9), together with the modified Coulomb friction law, given by (3.16). The radial clearance size is equal to 0.5 mm and four different values

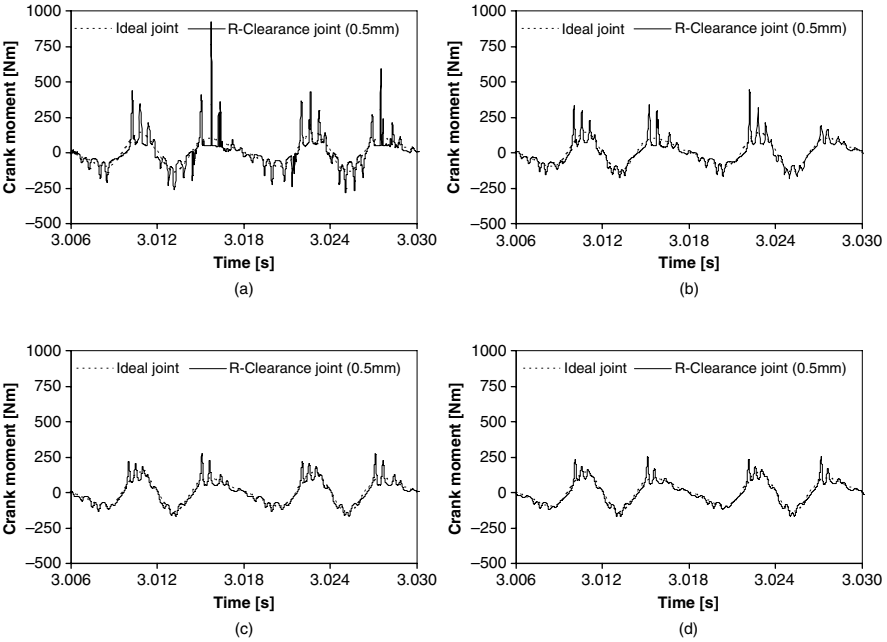

Fig. 4.19 Crank moment for different values of friction coefficient: (**a**) $c_f = 0.01$; (**b**) $c_f = 0.03$; (**c**) $c_f = 0.05$; (**d**) $c_f = 0.1$

for friction coefficient are used, namely, 0.01, 0.03, 0.05 and 0.1. Figure 4.19 depicts the crank moments for different friction coefficient values. The journal center trajectories and the corresponding Poincaré maps are shown in Figs. 4.20 and 4.21.

In general, the effect of the friction is to reduce the peaks of the force values due to the impact between the journal and the bearing. This can be observed in the crank moment plots, displayed in Fig. 4.19a–d. Figure 4.20a–d shows that the path of the journal center is characterized by a continuous contact, i.e., the journal follows the bearing wall all the time when the friction coefficient is increased. By observing Figures 4.19–4.21 it is clear that, when the friction coefficient increases, the dynamic response of the system tends to be periodic and closer to that of the system with ideal joints. For a low value of the friction coefficient, the system response is chaotic since the Poincaré map has the trajectories spread, as shown in Fig. 4.21a.

In short, multibody mechanical systems with clearance joints are well known as nonlinear dynamic systems that, under certain conditions, exhibit a chaotic response. However, from the results presented here, it is found that the dynamics of the revolute clearance joint in multibody mechanical systems is sensitive not only to the clearance size but also to the friction coefficient. With a small change in one of these parameters the response of the system can shift from chaotic to periodic and vice versa.

In what follows, several models demonstrate how different contact force models may influence the behavior of the slider–crank mechanism and what their

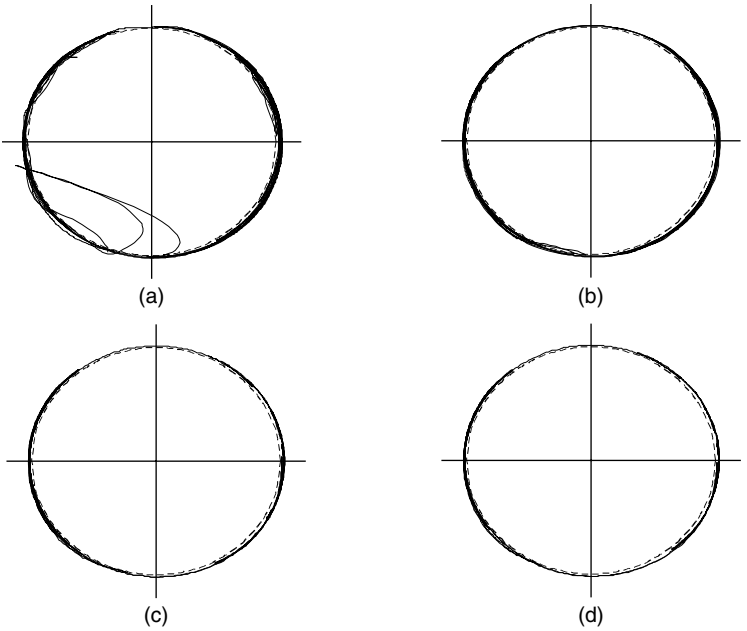

Fig. 4.20 Journal center trajectory for different values of friction coefficient: (**a**) $c_f = 0.01$; (**b**) $c_f = 0.03$; (**c**) $c_f = 0.05$; (**d**) $c_f = 0.1$

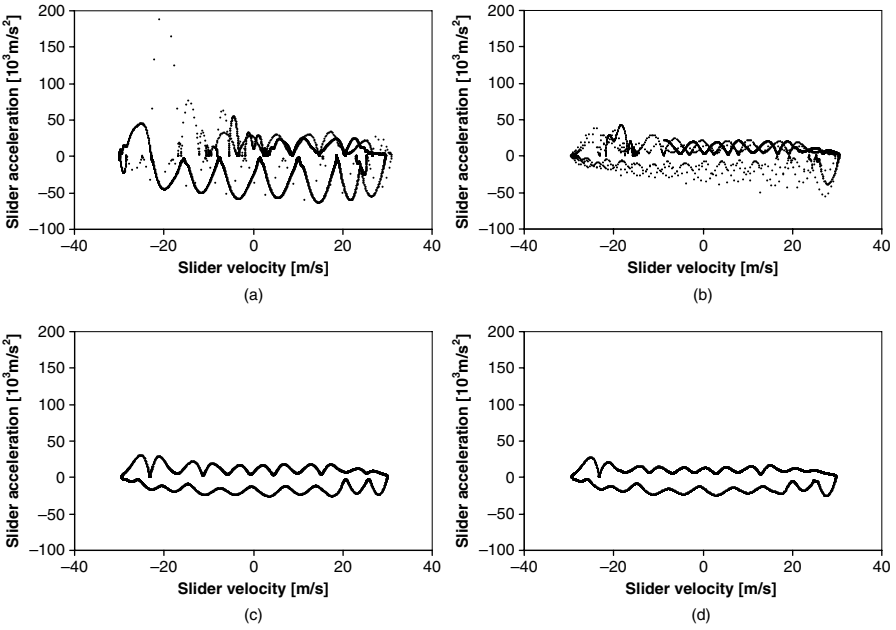

Fig. 4.21 Poincaré maps for different values of friction coefficient: (**a**) $c_f = 0.01$; (**b**) $c_f = 0.03$; (**c**) $c_f = 0.05$; (**d**) $c_f = 0.1$

consequences are in terms of the contact force and crank reaction moment. The contact force models for both spherical and cylindrical contact surfaces, presented in Chap. 3, are used here. The impact is treated as being frictionless and the radial clearance size is set to be 0.5 mm. The contact force for two full crank rotations is used to illustrate the behavior of the slider–crank mechanism, when different contact force models are applied. The contact forces corresponding to each model are pictured in Fig. 4.22. In addition to the contact force, the driving crank moment necessary to maintain a constant crank angular velocity for the different contact models and the journal center trajectories are presented in Figs. 4.23 and 4.24, respectively.

From Fig. 4.22, it is clear that for all pure elastic contact models the level of contact force is higher when compared to the continuous contact force model by

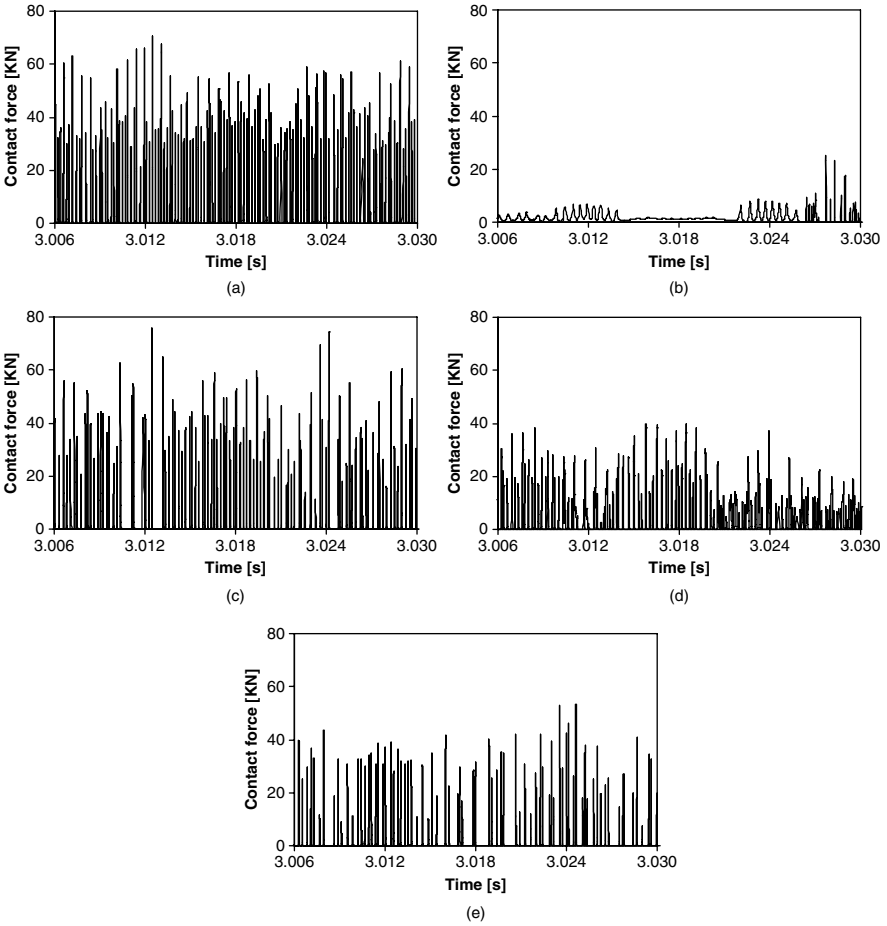

Fig. 4.22 Contact force between the journal and the bearing for the contact models presented: (**a**) Hertz contact law; (**b**) Lankarani and Nikravesh model; (**c**) Dubowsky and Freudenstein model; (**d**) Goldsmith model; (**e**) ESDU 78035 model

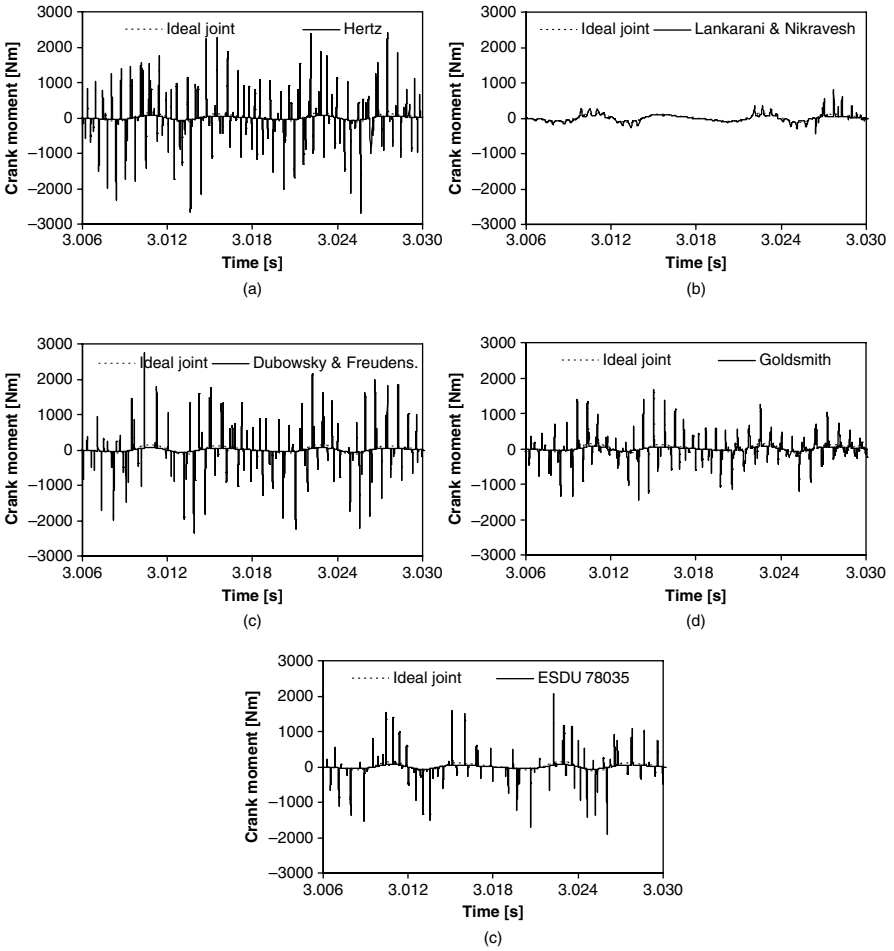

Fig. 4.23 Driving crank moment for the different contact models presented: (**a**) Hertz contact law; (**b**) Lankarani and Nikravesh model; (**c**) Dubowsky and Freudenstein model; (**d**) Goldsmith model; (**e**) ESDU 78035 model

Lankarani and Nikravesh (1990) with a restitution coefficient $c_e = 0.9$. A similar conclusion can be drawn from Fig. 4.23a–e, since the impact forces are propagated through the rigid bodies of the slider–crank mechanism. By inspecting Fig. 4.24a–e it is observed that the contact models, which do not include energy dissipation, have short periods of contact between the journal and the bearing and long free flight periods. The contact model given by (3.9), which accounts for energy dissipation, presents long periods of contact between the journal and the bearing.

In Fig. 4.24a–e, the journal trajectories are presented by continuous lines that connect points. A point is plotted for each integration time step and represented by a marker, the relative penetration depth being visible by points outside the clearance circle. The point density is very high when the journal contacts the bearing wall,

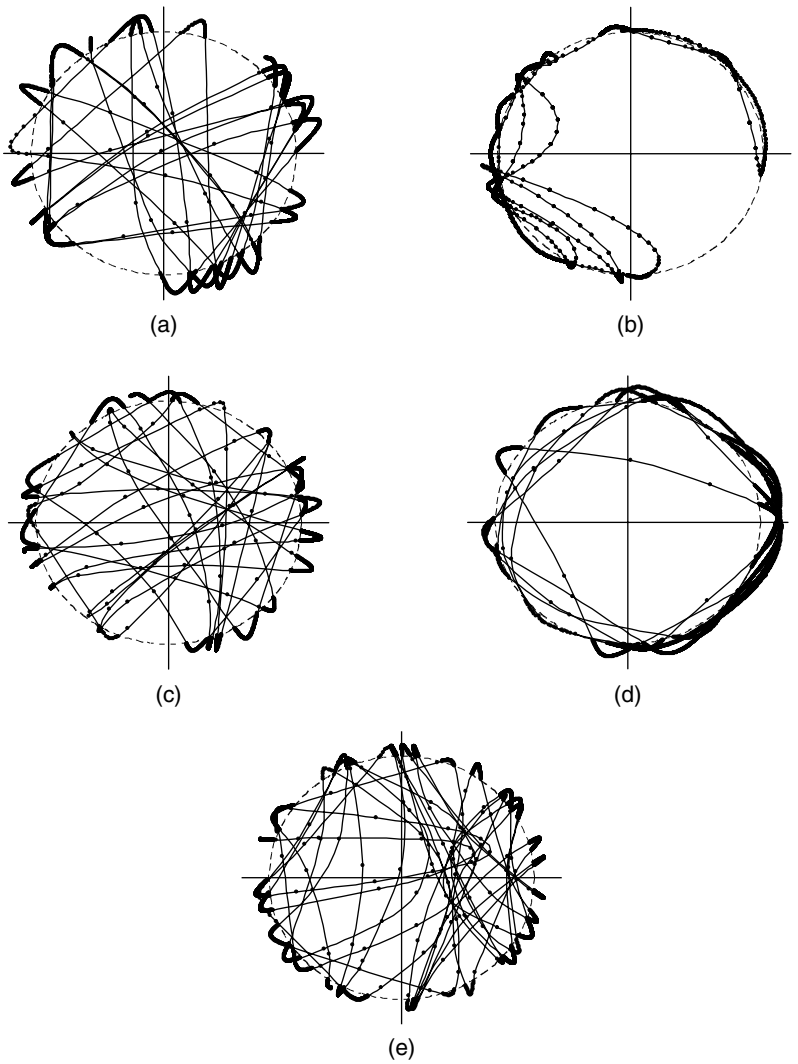

Fig. 4.24 Journal center trajectory for the different contact models: (**a**) Hertz contact law; (**b**) Lankarani and Nikravesh model; (**c**) Dubowsky and Freudenstein model; (**d**) Goldsmith model; (**e**) ESDU 78035 model

which means that the step size of the integration algorithm is small. When the journal is in free flight motion, the time step is automatically increased by the integration algorithm and, consequently, the points plotted in Fig. 4.24a–e are further apart. This shows the importance of using a varying time-step integration scheme for the dynamic analysis of systems that involve contact and impact.

Figure 4.25a–d depicts the influence of the coefficient of restitution on the crank moment when the continuous contact force model proposed by Lankarani and

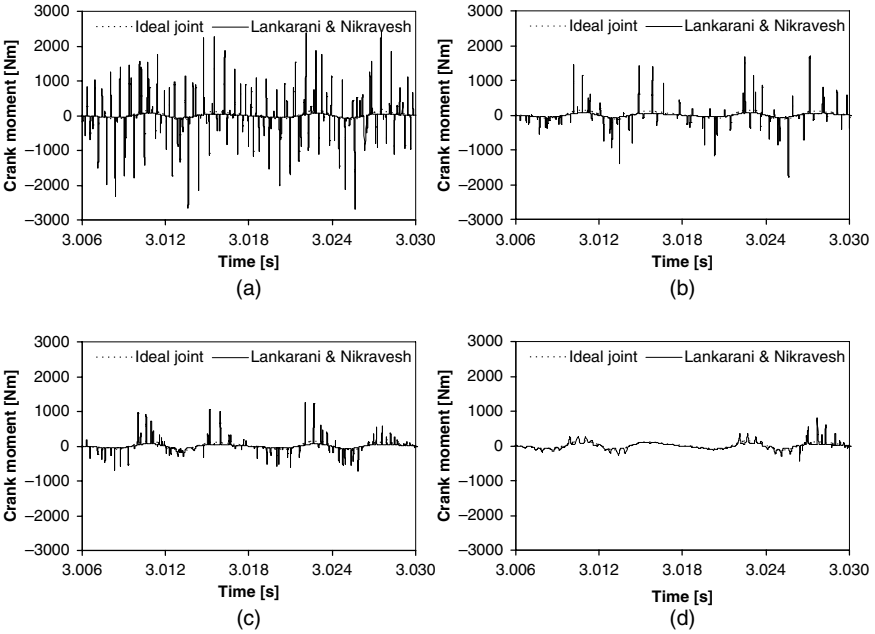

Fig. 4.25 Crank moment for different values of the restitution coefficient when the continuous contact force model proposed by Lankarani and Nikravesh (1990) is used: (**a**) $c_e = 1.00$; (**b**) $c_e = 0.99$; (**c**) $c_e = 0.95$; (**d**) $c_e = 0.90$

Nikravesh (1990), given by (3.9), is used. This model shows a direct relationship between the contact force and coefficient of restitution that is selected to the process of energy dissipation during the impact. In the case studies presented, the radial clearance size is equal to 0.5 mm and four different coefficients of restitution are selected, namely, 1.00, 0.99, 0.95 and 0.90. In Fig. 4.25a–e, it is observed that when the coefficient of restitution decreases, the peaks of the crank moment values are reduced, indicating a higher energy dissipation during the contact.

Figure 4.26a and b shows the time variation of the contact force and the relation between the force and penetration depth for different values of the coefficient of restitution, for the first impact only. Observing Fig. 4.26b, it is important to highlight how the hysteresis loop increases when the coefficient of restitution decreases. When the restitution coefficient is the unit, which corresponds to the pure Hertz contact force law, there is no energy dissipation in the contact process. This result is evident in the force-penetration depth relation of Fig. 4.26b, which does not present an hysteresis loop.

Some important conclusions can be drawn from the study presented here. Among the spherical shaped contact areas, the linear Kelvin–Voigt contact model does not represent the overall nonlinear nature of impact. The Hertz relation, besides its nonlinearity, does not account for the energy dissipation during the impact process. Therefore the Hertz relation along with the modification to represent the energy

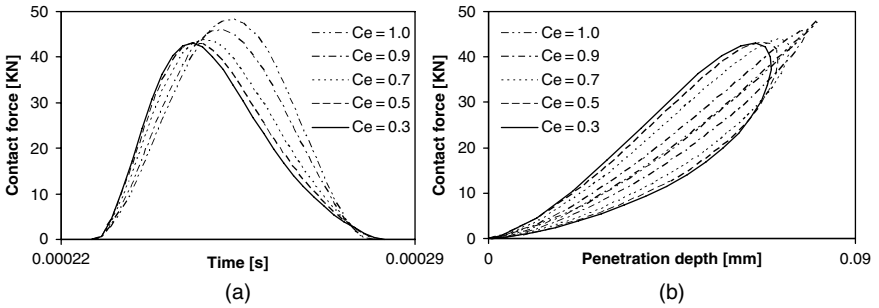

Fig. 4.26 Influence of the coefficient of restitution for the Lankarani and Nikravesh continuous contact force model: (**a**) contact force versus time; (**b**) force–penetration depth relation

dissipation in the form of internal damping is advantageous for modeling contact forces in a multibody system. The cylindrical models are expressed by nonlinear and implicit functions of penetration depth and they require a numerical iterative procedure to solve them, if no approximation is to be used.

The different continuous contact force models which use an elastic contact theory lead to comparable results in terms of contact forces, crank moments and journal trajectories. However, when dissipation is allowed to take place, the peaks of the crank moments that are required to drive the mechanism with a constant angular velocity are much lower than those observed for the elastic models. This observation is consistent with the comparisons of the flight trajectories observed for the different models. It was observed that the energy dissipation of the continuous contact model, proposed by Lankarani and Nikravesh (1990), results in long periods of time when the journal seats in the bearing, thus predicting a much smoother dynamic response of the system. Furthermore because the restitution coefficient plays a role in the control of the energy dissipation this model can represent a much broader number of contact conditions.

4.5 Application 2: Slider–Crank with Translational Clearance Joint

In order to examine the consequences of the formulation developed for the translational clearance joint, the planar slider–crank mechanism, discussed in the previous section, is considered again as a numerical example here. All joints are ideal except for the translation joint that has a clearance, as shown in Fig. 4.27. The translational clearance joint is composed of a guide and a slider. This joint has a finite clearance, which is constant along the length of the slider.

It is assumed that the crank is driven at a constant angular velocity equal to 5000 rpm, maintained by varying the input torque. Initially the slider is at the same distance from the upper and lower guide surfaces and the initial velocities and positions

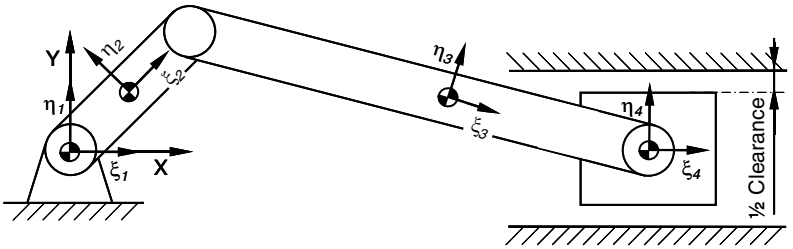

Fig. 4.27 Slider–crank mechanism with a translational clearance joint

are those used in Sect. 4.4. Table 4.3 shows the parameters used in the simulation of this demonstrative example.

The dynamic performance of the slider–crank mechanism study case is demonstrated through the time plots of the slider velocity and acceleration and the moment that acts on the crank, which are presented in Figure 4.28. Additionally the slider trajectories inside the guide are represented in Fig. 4.28 in a nondimensional plot. Results for two full crank rotations are given in Fig. 4.28a–d. The impact between the slider and guide surfaces is assumed to be frictionless, the Lankarani and Nikravesh contact force model expressed by (3.9) being used to compute the normal forces. For convenience, a small radius of curvature at each slider corner is considered, in order to calculate the equivalent generalized stiffness given by (3.5).

The slider velocities and acceleration, presented in Fig. 4.28a and b, clearly show the influence of the clearance in the kinematics of the translation joint. The slider velocity diagram is smooth and close to the ideal joint simulation. The smooth changes in the velocity also indicate that the slider and guide surfaces are in permanent contact for long periods. Some sudden changes in the velocity are due to the impacts between the slider and guide surfaces. These impacts are visible in the acceleration diagram by high values in the form of peaks in the response. Since the bodies of the slider–crank mechanism are rigid, the impact forces are propagated from the slider to the crank, leading to visible high peaks in the crank moment diagram shown in Fig. 4.28c.

The dimensionless slider trajectories are shown in Fig. 4.28d. There, the different types of motion between the slider and guide observed are associated with the different guide–slider configurations, that is, no contact, contact-impact followed by rebound and permanent contact. The dimensionless X-slider motion varies from

Table 4.3 Numerical parameters used in the dynamic simulation of the slider–crank mechanism with a translational clearance joint

Clearance size	0.5 mm	Young's modulus	207 GPa
Slider length	50.0 mm	Poisson's ratio	0.3
Slider width	50.0 mm	Baumgarte - α	5
Slider thickness	50.0 mm	Baumgarte - β	5
Corner curvature radius	1.0 mm	Integration step	10^{-5} s
Restitution coefficient	0.9	Integration tolerance	10^{-6} s

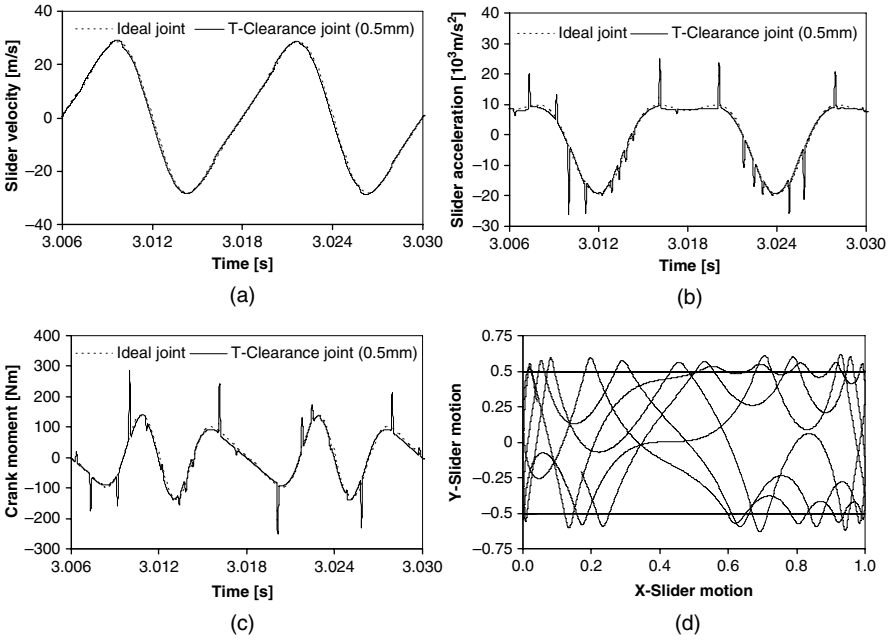

Fig. 4.28 (**a**) Slider velocity; (**b**) slider acceleration; (**c**) crank moment; (**d**) dimensionless slider trajectories inside the guide

0 to 1, which corresponds to the low and top dead ends, respectively. The dimensionless Y-slider motion higher than 0.5 corresponds to the case in which the slider and the upper guide surface are in contact, whereas the dimensionless Y-slider motion lower than −0.5 corresponds to the case in which the contact takes place between the slider and the lower guide surface. The horizontal lines in the slider path diagrams represent the geometric limits for contact situations between the slider and guides surfaces.

In order to understand the influence of the clearance size in the dynamic behavior of the slider–crank mechanism, the driving crank moment is plotted in Fig. 4.29a–d for simulations where the clearance in the translational clearance joint varies from 0.01 to 0.5 mm. In addition to the crank moment, the respective slider trajectories and the Poincaré maps are presented in Figs. 4.30 and 4.31. Again the slider acceleration and slider velocity are chosen to build the Poincaré maps.

From Fig. 4.29 it is evident that when the clearance size is small the crank moment peaks are lower and the dynamic response tends to be closer to the ideal translation joint case. This suggests that the periods of permanent contact between the slider and guide surfaces are longer and, hence, the slider and guide experiment fewer impacts. This observation can be confirmed by the slider trajectories and Poincaré maps provided in Figs. 4.30 and 4.31, respectively. When the clearance size is reduced, the system response changes from chaotic, as displayed in

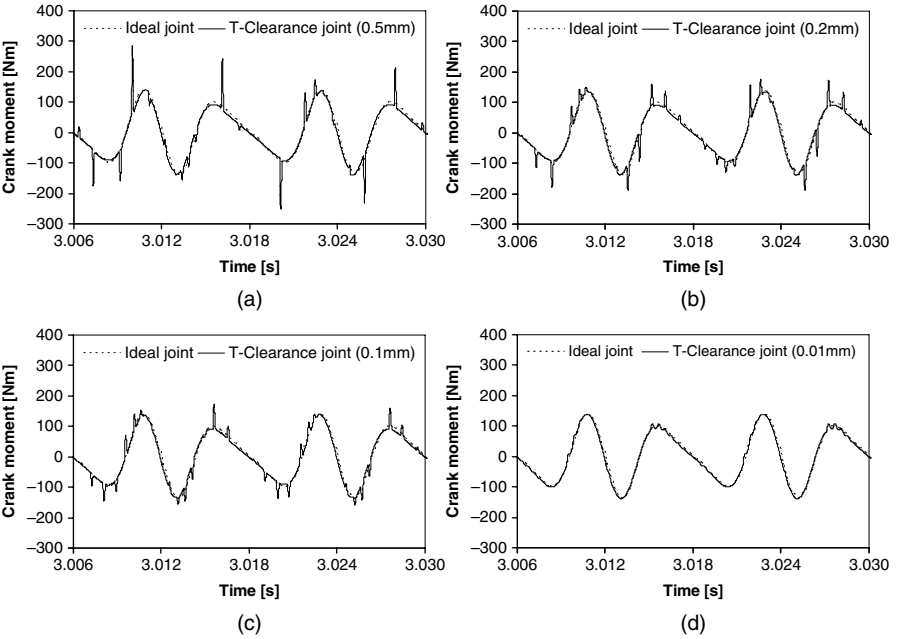

Fig. 4.29 Driving crank moment for different clearance sizes in the translational clearance joint: (**a**) $c = 0.5$ mm; (**b**) $c = 0.2$ mm; (**c**) $c = 0.1$ mm; (**d**) $c = 0.01$ mm

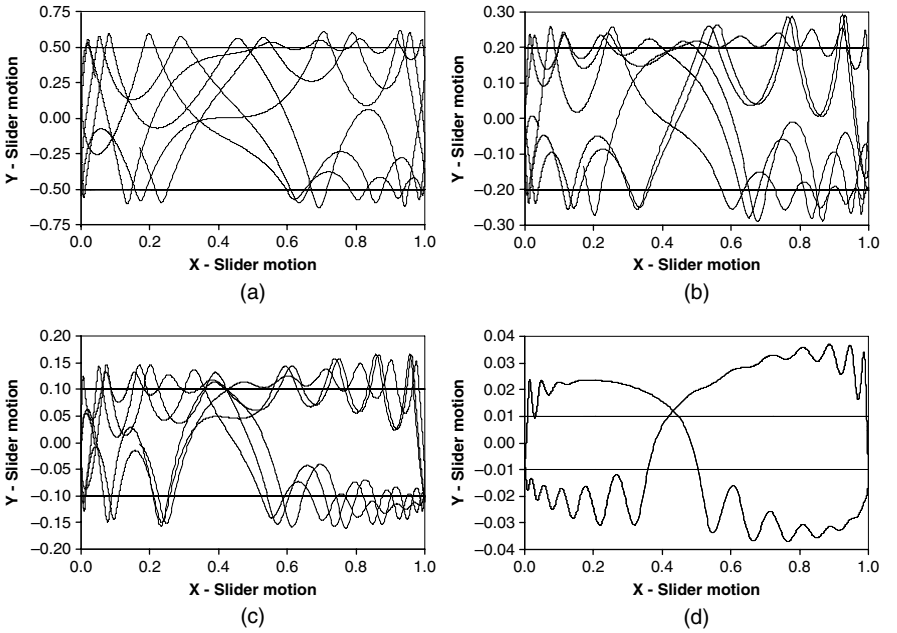

Fig. 4.30 Dimensionless slider path for different clearance sizes in the translational clearance joint: (**a**) $c = 0.5$ mm; (**b**) $c = 0.2$ mm; (**c**) $c = 0.1$ mm; (**d**) $c = 0.01$ mm

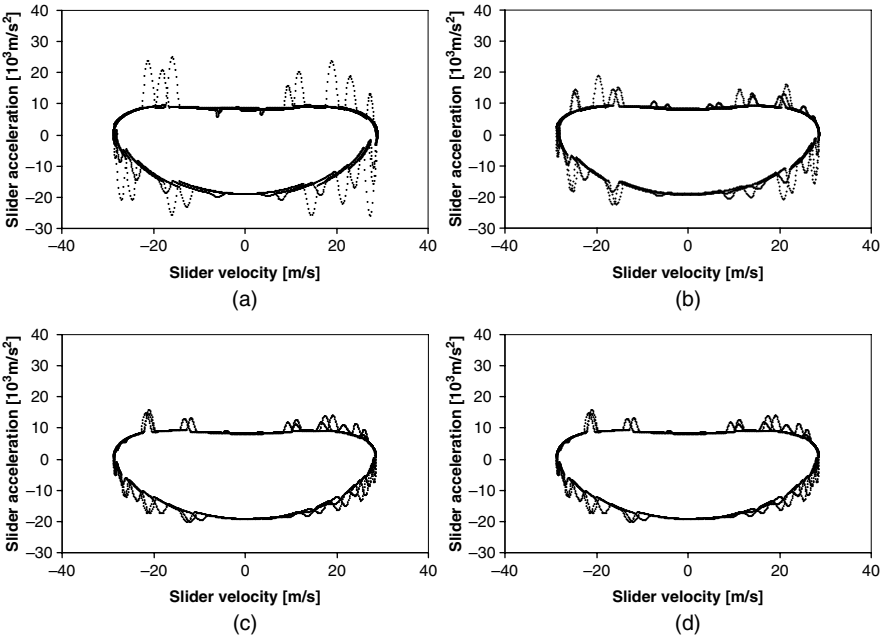

Fig. 4.31 Poincaré maps for different clearance sizes in the translational clearance joint: (**a**) $c = 0.5$ mm; (**b**) $c = 0.2$ mm; (**c**) $c = 0.1$ mm; (**d**) $c = 0.01$ mm

Fig. 4.30a, to periodic or regular, as observed in Fig. 4.31d. This feature can be useful in the evaluation of the acceptable range for clearance, in any type of construction where this type of joints is applied.

The effect of the friction phenomenon on the dynamic performance of the translational clearance joint is also studied. Again the driving crank moment, the slider path and Poincaré maps are used to quantify the dynamic response of the slider–crank mechanism and represented in Figs. 4.32–4.34. The value for the clearance size is equal to 0.5 mm in all simulations, and four different values for the friction coefficient are used, namely, 0.01, 0.03, 0.05 and 0.1.

In Fig. 4.32, it is observed that the reaction, or driving crank moment necessary to maintain constant crank angular velocity, does not relate directly to the friction coefficient value, that is, when the friction coefficient increases the peak values of the crank moment do not show tendency to increase or decrease. Analyzing the slider trajectories, plotted in Figs. 4.33a–d, and the corresponding Poincaré maps, shown in Fig. 4.34a–d, it is observed that the influence of the friction coefficient in global system response is not significant, conversely to what happens in the case of the revolute clearance joint, shown in Figs. 4.19–4.21.

The influence of employing different contact force models on the global slider–crank behavior is also analyzed in this work. Figures 4.35 and 4.36 show the contact forces and driving crank moments for the contact force models given by (3.9) and (4.26), respectively, that is, the nonlinear force model proposed by Lankarani and

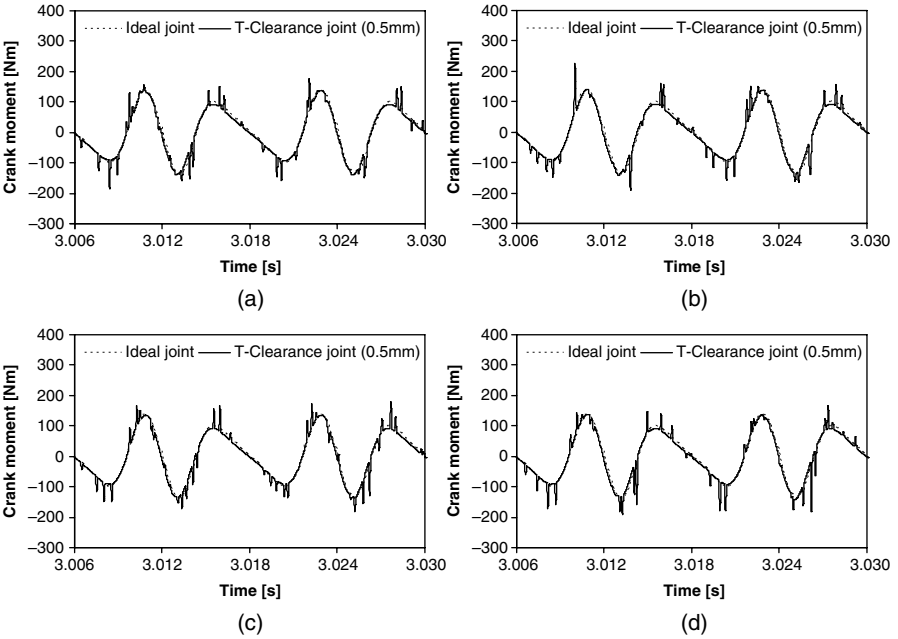

Fig. 4.32 Driving crank moment for different values of the friction coefficient in the translational clearance joint: (**a**) $c_f = 0.01$; (**b**) $c_f = 0.03$; (**c**) $c_f = 0.05$; (**d**) $c_f = 0.1$

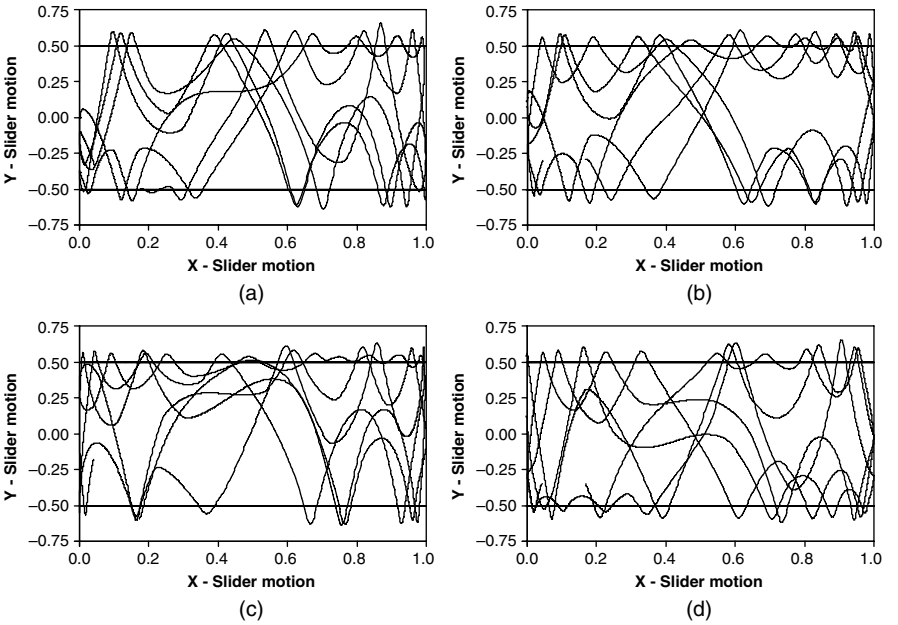

Fig. 4.33 Slider path for different values of the friction coefficient in the translational clearance joint: (**a**) $c_f = 0.01$; (**b**) $c_f = 0.03$; (**c**) $c_f = 0.05$; (**d**) $c_f = 0.1$

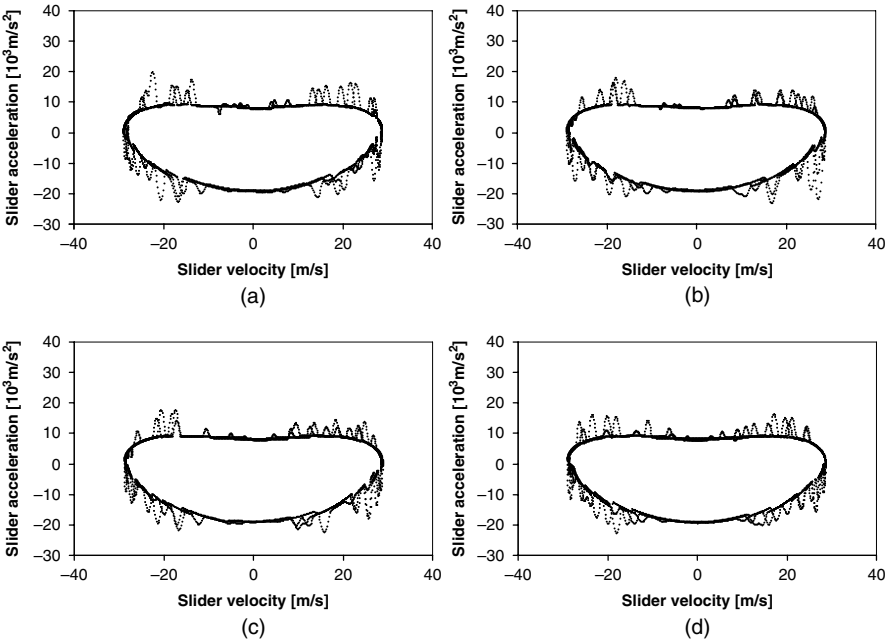

Fig. 4.34 Poincaré maps for different friction coefficients in the translational clearance joint: (**a**) $c_f = 0.01$; (**b**) $c_f = 0.03$; (**c**) $c_f = 0.05$; (**d**) $c_f = 0.1$

Nikravesh (1990), using a restitution coefficient of $c_e = 0.9$, and the linear force model for two plane surfaces presented by Lankarani (1988). In the case of the linear contact model for two plane surfaces, the average penetration is used to evaluate the magnitude of the contact force. This force is then applied at the geometric center of the penetration area, as schematically shown in Fig. 4.11a.

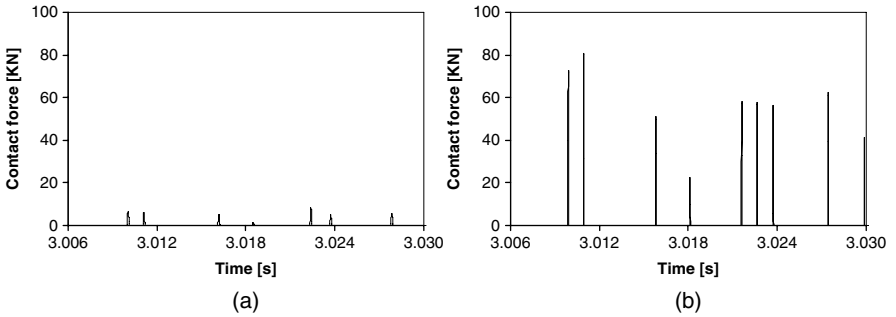

Fig. 4.35 Contact force between the slider and guide surface: (**a**) Lankarani and Nikravesh model; (**b**) linear contact model for two plane surfaces

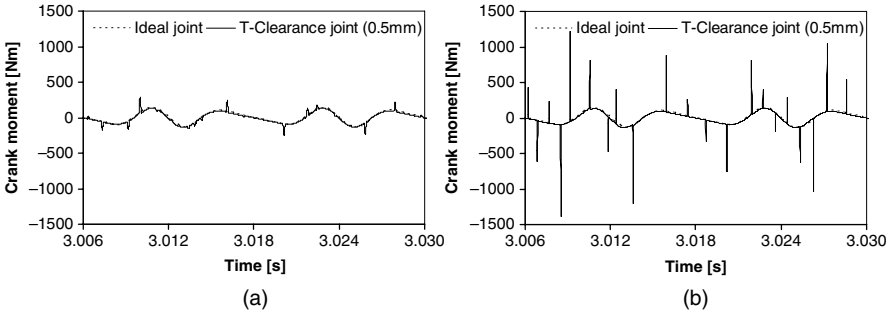

Fig. 4.36 Driving crank moment: (**a**) Lankarani and Nikravesh model; (**b**) linear contact model for two plane surfaces

4.6 Summary

A comprehensive approach to the modeling of unlubricated clearance joints in planar multibody systems has been presented in this chapter, with specialization for the revolute and translational joints. In the process, different contact models have been revised in face of their suitability to represent the impact between the bodies joined by these joints. The methodologies proposed have been exemplified, through the application to the dynamic study of a slider–crank mechanism with revolute and translational clearance joints.

A critical aspect, in the precise prediction of the peak forces, is the proper selection of an appropriate contact model. From the comparison between the cylindrical contact force models and spherical contact force models, one can conclude that the spherical and cylindrical force–displacement relations are reasonably close. Furthermore the straightforward force–penetration relation proposed by Lankarani and Nikravesh (1990) is largely used for mechanical contacts owing to its simplicity and easiness of implementation in a computational program and also because this is the only model that accounts for energy dissipation during the impact process. A modified Coulomb's friction law was used to model the friction phenomenon; one merit of this modified model is that it improves the numerical stability of the integration algorithm.

How the solution strategy of the contact problem associated with the modeling of joints with clearances is sensitive to the procedure used to detect contact was discussed. In the sequel of the techniques proposed, a numerical strategy that takes advantage of the use of a variable time-step integration algorithm has been proposed to handle the identification of the start of contact and to proceed afterwards.

The dynamic response of the slider–crank mechanism with clearance joints, in terms of Poincaré maps, shows that periodic and nonperiodic responses can occur. Poincaré maps play a key role in representing the global behavior of dynamical systems. For the radial clearance and friction coefficient values used in this work the system response exhibits both periodic and chaotic responses. When the clearance is reduced, the dynamic response changes from chaotic to periodic or regular behavior.

In fact, most of the mechanical systems present some inherent nonlinearity even when modeled with ideal joints. The chaotic behavior of the mechanical system may be eliminated with suitable design and/or parameter changes of mechanical system.

For the case of revolute clearance joint analysis, the overall results are corroborated by published works on this field, for cases that include dry contact force models (Ravn 1998, Schwab 2002). The results for translational clearance joints in mechanical systems seem quite acceptable, but they cannot be compared with other results since this issue has not been addressed before in the literature.

The planar slider–crank mechanism with a translational clearance joint was used as a numerical example to illustrate the methodology proposed. In general, the dynamic response of the slider–crank mechanism presents some peaks, due to the impact between the slider and the guide, namely in what concerns the accelerations and reaction moments. It was observed that all curves for the kinematic and kinetic variables are similar to those obtained with ideal joints, with the exception of the peaks especially visible for the forces and accelerations. These peaks have been clearly associated to the existence of the clearances and to their magnitude. The relative motion between the guide and slider showed a very high nonlinearity, or even chaotic behavior, when a translational clearance is included. When the clearance size is reduced, the system's response becomes closer to the case for ideal joints. Furthermore the dynamic behavior of the slider–crank model tends to be periodic or regular. This feature can be useful in calculations of an acceptable range for the clearance, during the design process.

The conclusions drawn from the results presented in this chapter must be considered in the light of the assumptions identified in the formulation of the motion's equation, namely the assumption of rigidity for the bodies, the lack of joints' flexibility and the nonexistence of lubrication effects. In this chapter, contact between the surfaces that constitute the clearance joints was assumed to be dry, i.e., without any interposition fluid layer. Consequently contact-impact forces and friction forces were the only loads on the contacting bodies when the physical contact was detected between the surfaces. In the engineering design of machines and mechanisms, journal–bearings are usually designed to operate with some lubricant. Lubricated journal–bearings are designed so that when the maximum load is applied, the journal and bearing do not come into contact. The main reason for designing journal–bearings in this way is to reduce the friction and extend the lifetime of mechanical systems. The issue of lubricated journal–bearings in mechanical systems is presented and discussed in the next chapter.

References

Ambrósio JAC (2002) Impact of rigid and flexible multibody systems: deformation description and contact models. Virtual nonlinear multibody systems, NATO Advanced Study Institute, Prague, Czech Republic, June 23–July 3, edited by W Schiehlen and M Valásek, Vol. II, pp. 15–33.

Baker GJ, Gollub JP (1990) Chaotic dynamics—an introduction. Cambridge University Press, Cambridge, United Kingdom.

Bauchau OA, Rodriguez J (2002) Modelling of joints with clearance in flexible multibody systems. International Journal of Solids and Structures 39:41–63.
Bengisu MT, Hidayetoglu T, Akay A (1986) A theoretical and experimental investigation of contact loss in the clearances of a four-bar mechanism. Journal of Mechanisms, Transmissions, and Automation in Design 108:237–244.
Dubowsky S (1974) On predicting the dynamic effects of clearances in planar mechanisms. Journal of Engineering for Industry, Series B 96(1):317–323.
Dubowsky S, Freudenstein F (1971a) Dynamic analysis of mechanical systems with clearances, part 1: formulation of dynamic model. Journal of Engineering for Industry, Series B 93(1):305–309.
Dubowsky S, Freudenstein F (1971b) Dynamic analysis of mechanical systems with clearances, part 2: dynamic response. Journal of Engineering for Industry, Series B 93(1):310–316.
Earles SWE, Wu CLS (1975) Predicting the occurrence of contact loss and impact at the bearing from a zero-clearance analysis. Proceedings of IFToMM fourth world congress on the theory of machines and mechanisms, Newcastle Upon Tyne, England, pp. 1013–1018.
Farahanchi F, Shaw, SW (1994) Chaotic and periodic dynamics of a slider crank mechanism with slider clearance. Journal of Sound and Vibration 177(3):307–324.
Flores P, Ambrósio J (2004) Revolute joints with clearance in multibody systems. Computers and Structures, Special Issue: Computational Mechanics in Portugal 82(17–18):1359–1369.
Flores P, Ambrósio J, Claro JCP, Lankarani HM, Koshy CS (2006) A study on dynamics of mechanical systems including joints with clearance and lubrication. Mechanism and Machine Theory 41(3):247–261.
Hertz H (1896) On the contact of solids—on the contact of rigid elastic solids and on hardness. Miscellaneous papers (Translated by DE Jones and GA Schott), pp. 146–183. Macmillan, London, England.
Lankarani HM (1988) Canonical equations of motion and estimation of parameters in the analysis of impact problems. Ph.D. Dissertation, University of Arizona, Tucson, AZ.
Lankarani HM, Nikravesh PE (1990) A contact force model with hysteresis damping for impact analysis of multibody systems. Journal of Mechanical Design 112:369–376.
Mansour WM, Townsend MA (1975) Impact spectra and intensities for high-speed mechanisms. Journal of Engineering for Industry, Series B 97(2):347–353.
Miedema B, Mansour WM (1976) Mechanical joints with clearance: a three mode model. Journal of Engineering for Industry 98(4):1319–1323.
Nikravesh PE (1988) Computer-aided analysis of mechanical systems. Prentice Hall, Englewood Cliffs, NJ.
Ravn P (1998) A continuous analysis method for planar multibody systems with joint clearance. Multibody System Dynamics 2:1–24.
Schwab AL (2002) Dynamics of flexible multibody systems, small vibrations superimposed on a general rigid body motion. Ph.D. Dissertation, Delft University of Technology, Netherlands.
Shabana AA (1989) Dynamics of multibody systems. Wiley, New York.
Thümmel T, Funk K (1999) Multibody modelling of linkage mechanisms including friction, clearance and impact. Proceedings of tenth world congress on the theory of machine and mechanisms, Oulu University, Finland, Vol. 4, pp. 1375–1386.
Timoshenko SP, Goodier JN (1970) Theory of elasticity. McGraw-Hill, New York.
Tomsen JJ (1997) Vibrations and stability—order and chaos, McGraw-Hill, New York.
Townsend MA, Mansour WM (1975) A pendulating model for mechanisms with clearances in the revolutes. Journal of Engineering for Industry, Series B 97(2):354–358.
Wiggins S (1990) Introduction to applied nonlinear dynamical systems and chaos. Springer Berlin Heidelberg New York.
Wilson R, Fawcett JN (1974) Dynamics of slider–crank mechanism with clearance in the sliding bearing. Mechanism and Machine Theory 9:61–80.
Wu CLS, Earles SWE (1977) A determination of contact-loss at a bearing of a linkage mechanism. Journal of Engineering for Industry, Series B 99(2):375–380.
Zukas JA, Nicholas T, Greszczuk LB, Curran DR (1982) Impact dynamics. Wiley, New York.